

## Diagnostics from three rising submillimeter bursts

Ai-Hua Zhou<sup>1,2</sup>, Jian-Ping Li<sup>1,2</sup> and Xin-Dong Wang<sup>3</sup>

<sup>1</sup> Key Laboratory of Dark Matter and Space Astronomy, Chinese Academy of Sciences, Nanjing 210008, China; zhouah@pmo.ac.cn

<sup>2</sup> Purple Mountain Observatory, Chinese Academy of Sciences, Nanjing 210008, China

<sup>3</sup> School of Public Administration, Hohai University, Nanjing 210098, China

Received 2015 July 1; accepted 2015 September 10

**Abstract** In this paper we investigate three novel rising submillimeter (THz) bursts that occurred sequentially in Super Active Region NOAA 10486. The average rising rate of the flux density above 200 GHz is only 20 sfu GHz<sup>-1</sup> (corresponding to spectral index  $\alpha$  of 1.6) for the THz spectral components of the 2003 October 28 and November 4 bursts, but it attained values of 235 sfu GHz<sup>-1</sup> ( $\alpha = 4.8$ ) in the 2003 November 2 burst. The steeply rising THz spectrum can be produced by a population of highly relativistic electrons with a low-energy cutoff of 1 MeV, but it only requires a low-energy cutoff of 30 keV for the two slowly rising THz bursts, via gyrosynchrotron (GS) radiation based on our numerical simulations of burst spectra in the magnetic dipole field case. The electron density variation is much larger in the THz source than in the microwave (MW) source. It is interesting that the THz source radius decreased by 20%–50% during the decay phase for the three events, but the MW source increased by 28% for the 2003 November 2 event. In the paper we will present a formula that can be used to calculate the energy released by ultrarelativistic electrons, taking the relativistic correction into account for the first time. We find that the energy released by energetic electrons in the THz source exceeds that in the MW source due to the strong GS radiation loss in the THz range, although the modeled THz source area is 3–4 orders smaller than the modeled MW source one. The total energies released by energetic electrons via the GS radiation in radio sources are estimated, respectively, to be  $5.2 \times 10^{33}$ ,  $3.9 \times 10^{33}$  and  $3.7 \times 10^{32}$  erg for the October 28, November 2 and 4 bursts, which are 131, 76 and 4 times as large as the thermal energies of  $2.9 \times 10^{31}$ ,  $2.1 \times 10^{31}$  and  $5.2 \times 10^{31}$  erg estimated from soft X-ray GOES observations.

**Key words:** Sun: submillimeter emission — Sun: energetic electrons — Sun: radio source environment

### 1 INTRODUCTION

Solar flares are a consequence of magnetic instabilities in solar flare regions. During the flares, a large amount of magnetic energy is converted into the acceleration of charged particles. A broad spectrum of electromagnetic radiation is emitted. So, one of the most direct diagnostics of energetic ( $\sim 1$  MeV) electrons accelerated during solar flares is their gyrosynchrotron (GS) radiation at centimeter-millimeter wavelengths emitted in magnetic loops associated with the flaring active region (AR) (e.g., Pick et al. 1990; Bastian et al. 1998). Before the year 2000, no radio observations above 90 GHz were available. At such frequencies the characteristic energy of radiating electrons is of order a few MeV (e.g., Dulk 1985; Ramaty et al. 1994). Since 2000, new instrumentation for observing in the 200–400 GHz range has become available, and more than 10 flares have been observed in this band (Lüthi et al. 2004a,b; Silva et al. 2007; Krucker et al. 2013).

It is interesting that among them, three strong submillimeter bursts occurred in succession in the same Super

AR NOAA 10486 on 2003 October 28 and November 2 and 4. For the three events, none of the radio spectra above 200 GHz were the continuation of the GS spectrum measured at lower frequencies, but surprisingly they showed increases with increasing frequency (Lüthi et al. 2004a; Kaufmann et al. 2004; Silva et al. 2007; Trotter et al. 2008). This spectral feature is termed a “THz component.” The positive-slope THz bursts have been observed thus far in only a handful of the most energetic events (Krucker et al. 2013). So, the three THz burst observations that occurred in the same AR are very valuable for understanding this process.

The THz wavelength range (0.1–10 THz) is a frontier observational window and its role is special compared to other wavelength ranges, because it can provide unique diagnostics about energy release in ultrarelativistic electrons and their environment in lower levels of the atmosphere from 1000 to 30 000 km above the photosphere in flare regions. The THz events that occurred on 2003 November 4 and 2 have been studied briefly (Zhou et al. 2010, 2011). In this paper we will investigate the 2003 October 28 event in

detail. We carried out a series of numerical simulations for the spectral observations, using our GS emission model in the case of a magnetic dipole field (Zhou et al. 2008).

In this paper we will present, for the first time, a formula that can be used to calculate the energy released by energetic electrons in the THz emission region, including the relativistic correction. We will use it to obtain an estimation of the energy released by energetic electrons in THz and microwave (MW) emission regions for the three THz events. The total non-thermal energy released by energetic electrons in the radio wavelength range and thermal energy estimated from the soft X-ray GOES observations are estimated and compared for the three bursts. Finally, we present discussions and conclusions.

## 2 OBSERVATIONS

Extensive flare activities were observed in a Super AR NOAA 10486 during its disk passage that occurred on 2003 October 22 – November 4. Among them an extremely energetic 4B/X17.2 flare on 2003 October 28/11:10 was observed when the Super AR was located at S16 E08, i.e., close to the disk-center. The flare was rated the third largest X-ray flare recorded by the GOES satellite and the largest optical class (4B) flare observed so far. It was associated with a large MW burst and a rising THz burst. Emission at 210 GHz was first detected by the Köln Observatory for Submillimeter and Millimeter Astronomy (KOSMA) as a slow rise in intensity at  $\sim 11:00$  UT (Lüthi et al. 2004a; Trotter et al. 2008), i.e., ten minutes before at the onset of the flare. After a dramatic increase at  $\sim 11:02:30$  UT, enormous peak flux densities of 25 000 and 11 000 sfu were reached at 11:05:25 UT at 90 and 210 GHz respectively (see Fig. 1).

The second rising THz burst in Super AR 10486 was detected by the Solar Submillimeter Telescope (SST) at 212 and 405 GHz (Silva et al. 2007) in the flare on 2003 November 2 starting at  $\sim 17:16$  UT. This flare is classified as an X8.3 and 2B event. Their peak flux densities reached values of about 4000 and 70 000 sfu at 212 and 405 GHz respectively. When the Super AR passed the west limb of the solar disk, the third large rising THz burst was observed by SST on 2003 November 4/19:42 UT (Kaufmann et al. 2004). It was associated with an  $X_{\geq 28}$  flare, which was the largest X-ray event since observations began in 1976 (Kane et al. 2005). The peak flux densities at 18 and 212 GHz attained, respectively, values of 48 000 and 11 500 sfu at the maximum phase (see Table 1).

## 3 RISING RATE OF FLUX DENSITY IN THE SUBMILLIMETER SPECTRUM

For the rising THz burst on October 28, emission at 210 GHz was detected as a slow rise in intensity at  $\sim 11:00$  UT. The total flux density time profile exhibits a slowly varying, time-extended component from an extended source and a short-lived component from a compact source exhibiting three distinctive peaks. However there

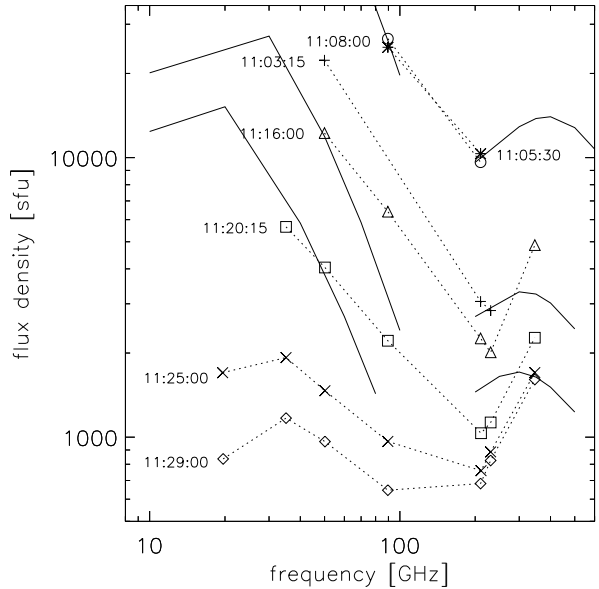


**Fig. 1** The temporal evolutions of radio spectra of the October 28 burst given by Lüthi et al. (2004a) and their associated fits (see the solid lines).

are no significant differences between the spectra emitted by the extended and the compact sources (Lüthi et al. 2004a). The flux density at 210 GHz increased from 3100 to 11 000 sfu in a period from 11:03:15 to 11:05:25 UT at the rise phase, but the 230 and 345 GHz KOSMA channels were saturated at these times due to the enormous flux density of the burst. So, the corresponding flux densities have not been recorded at 230/345 GHz during the main phase. Figure 1 shows the temporal evolution spectra of this event given by Lüthi et al. (2004a).

The rise rate  $r$  of the flux density measured from the observed spectra is in the  $18.5\text{--}8.5$  sfu GHz $^{-1}$  range during the October 28 burst (see Table 2), i.e., it is a slowly rising THz burst. The second THz burst occurred on November 4, exhibiting four peaks. Its rising rates of flux density are also given in Table 2. It shows that for the 2003 November 4 event, variation of the  $r$  value is in the range  $7.8\text{--}44$  sfu GHz $^{-1}$ , which means that it is also a slowly rising THz burst. Their average rising rate only reaches  $20$  sfu GHz $^{-1}$  (corresponding to a spectral index  $\alpha$  of 1.6) for the two events. The rising rates of the steeply rising THz burst from the 2003 November 2 event were estimated (Li et al. 2016). Its average rise rate could attain a value of  $235$  sfu GHz $^{-1}$  ( $\alpha=4.8$ ) for the 2003 November 2 burst, which is about one order of magnitude higher than that for the two slowly rising THz bursts.

## 4 FITS OF THE THREE RISING SUBMILLIMETER BURST SPECTRA

It is well known that the radio spectrum can provide crucial information about energetic electrons and their environment in solar flares. This information mainly contains

**Table 1** Three Novel Rising THz Burst Observations in the Super AR 10486

Date	H $\alpha$	X-ray	Position	$S_{\text{MW}}$ (sfu)	$S_{\sim 200 \text{ GHz}}$ (sfu)	$S_{405 \text{ GHz}}$ (sfu)
10 28 2003/11:02	4B	X <sub>17.2</sub>	S16E08	$S_{90 \text{ GHz}} : 25\,000$	11000	
11 02 2003/17:16	2B	X <sub>8.3</sub>	S18W56	$S_{18 \text{ GHz}} : 35\,000$	4000	70 000
11 04 2003/19:42	3B	X <sub>&gt;28</sub>	S19W83	$S_{18 \text{ GHz}} : 48\,000$	11 500	20 000

**Table 2** Rising Rates  $r$  (sfu GHz<sup>-1</sup>) of the Flux Density of the THz Component at the Rise, Maximum and Decay Phases for the Three THz Bursts, Measured from the Observations at 210 and 230/345 GHz (KOSMA), and at 212 and 405 GHz (SST).

Date	Time	Rise phase	Max. phase	Decay phase	$S_{\sim 200 \text{ GHz}}$	$S_{345\text{or}405 \text{ GHz}}$	$r$ (sfu GHz <sup>-1</sup> )
2003 10 28	11 : 03 : 15	yes			$3.1 \times 10^3$		
	11 : 05 : 30		yes		$1.1 \times 10^4$		
	11 : 16 : 00			yes	$2.2 \times 10^3$	$4.7 \times 10^3$	18.5
	11 : 20 : 15			yes	$1.2 \times 10^3$	$2.3 \times 10^3$	8.5
	11 : 25 : 00			yes	$8.5 \times 10^2$	$2.7 \times 10^3$	13.7
2003 11 02	11 : 29 : 00			yes	$8.0 \times 10^2$	$2.6 \times 10^3$	13.3
	17 : 16 : 15	yes			$1.2 \times 10^3$	$3.1 \times 10^4$	154
	17 : 17 : 06		yes		$4.0 \times 10^3$	$7.0 \times 10^4$	342
	17 : 17 : 30			yes	$3.2 \times 10^3$	$5.0 \times 10^4$	242
	17 : 18 : 00			yes	$3.5 \times 10^3$	$4.0 \times 10^4$	210
	17 : 18 : 30			yes	$4.0 \times 10^3$	$5.8 \times 10^4$	280
	17 : 19 : 00			yes	$5.0 \times 10^3$	$5.5 \times 10^4$	259
	17 : 19 : 30			yes	$5.0 \times 10^3$	$5.5 \times 10^4$	259
	17 : 20 : 00			yes	$5.0 \times 10^3$	$4.8 \times 10^4$	223
	17 : 21 : 00			yes	$4.5 \times 10^3$	$3.2 \times 10^4$	142
2003 11 04	19 : 42 : 40	yes			$2 \times 10^3$	$5 \times 10^3$	15.5
Peak 1	19 : 44 : 05		yes		$1.15 \times 10^4$	$2.0 \times 10^4$	44
Peak 2	19 : 45 : 20			yes	$10^4$	$1.65 \times 10^4$	33.7
Peak 3	19 : 46 : 50			yes	$10^4$	$1.5 \times 10^4$	25.9
Peak 4	19 : 48 : 25			yes	$3.7 \times 10^3$	$5.2 \times 10^3$	7.8

the energy spectral index  $\delta$ , low-energy and high-energy cutoffs  $E_0$  and  $E_m$  respectively, electron number density  $N$ , source size and magnetic field strength  $B$  in the source region.

#### 4.1 For the Two Slowly Rising THz Bursts

Here we will model the slowly rising THz spectral components of the 2003 October 28 burst for the first time. For this rising THz burst, the flux density at 210 GHz increased from 3100 to 11 000 sfu at the rise phase but the corresponding higher frequency ( $\nu > 210$  GHz) observations have not been obtained during the main phase. So we can only estimate the minimal conditions that could produce the rising THz spectral component with a 11 000 sfu flux density at 210 GHz at the maximum phase via the GS emission, which leads to the modeled spectrum being largely underestimated. It is well known that the low-energy cutoff and electron density can substantially affect the spectral calculations, so we selected, respectively, a sequence of low-energy cutoffs  $E_0$  and a sequence of electron number densities  $N$  to model the THz burst spectra for  $E_m = 10$  MeV. We find from these spectral calculations that the best set of values for the THz burst spectral fit at 11:05:30 UT of the maximum phase are for the low-energy cutoff of 30 keV and the number density of  $4.5 \times 10^{10} \text{ cm}^{-3}$ , where  $\delta=2$ ,  $B_0 = 5000$  G,  $\theta = 10^\circ$  and  $h_d = 10^8$  cm. The other two THz spectra at 11:16:00 and 11:20:15 UT at the decay phase are also fitted. The modeled THz and

MW emission spectra are given in Figure 1 in the case of a magnetic dipole field, which are superimposed on the original figure 10 (dotted lines) given by Lüthi et al. (2004a). It is shown that the modeled spectra agree well with the observational ones from the October 28 burst at 11:05:30, 11:08:00, 11:16:00 and 11:20:15 UT (see the solid lines). The physical parameters used in the spectral calculations are given in Table 3. We can find from Table 3 that during the THz burst, the required number density of electrons decreased substantially from  $4.5 \times 10^{10}$  to  $4.5 \times 10^8 \text{ cm}^{-3}$  at the decay phase. The fit results for the MW spectra of the October 28 burst are also given in Table 3 during the burst for  $E_0 = 10$  keV and  $E_m = 5$  MeV. At the decay phase, the electron number density  $N$  in the MW source decreased from  $6 \times 10^7$  to  $1.5 \times 10^6 \text{ cm}^{-3}$ , i.e., decreased by 40 times, but the value of  $N$  decreased by 100 times in the THz source. The total electron number  $N_{\text{total}}$  decreased by  $\sim 40$  and  $\sim 400$  times in the MW and THz sources, respectively.

Another slowly rising THz burst on November 4 was associated with the largest soft X-ray burst ( $X_{\geq 28}$ ) so far. However the associated rising THz spectral components are not so strong and the rising rates are only in the range 7.8–44 THz (see Table 1), so it is also identified as a slowly rising THz burst. The results of their spectral fit for peak 1 and peak 4 have been published (see the original fig. 2 and table 2 in Zhou et al. 2011). The required high-energy cutoff is also only 30 keV for the 2003 October 28 THz burst. The flux density reaches 11 500 sfu at 212 GHz for peak

**Table 3** Physical Parameters of Energetic Electrons for the Three Bursts

Date	Time	$\delta$	MW: $R''$	$N$ ( $\text{cm}^{-3}$ )	$N_{\text{total}}$	THz: $R''$	$N$ ( $\text{cm}^{-3}$ )	$N_{\text{total}}$
2003 10 28	11:05:30	2	25	$6.0 \times 10^7$	$2.0 \times 10^{35}$	0.5	$4.5 \times 10^{10}$	$5.9 \times 10^{34}$
	11:16:00	2.2	25	$2.0 \times 10^7$	$6.6 \times 10^{34}$	0.35	$6 \times 10^9$	$3.8 \times 10^{33}$
	11:20:15	1.9	25	$1.5 \times 10^6$	$4.9 \times 10^{33}$	0.25	$4.5 \times 10^8$	$1.5 \times 10^{32}$
2003 11 2	17:16:15	3	25	$8.0 \times 10^7$	$2.6 \times 10^{35}$	0.5	$8 \times 10^6$	$1.0 \times 10^{31}$
	17:17:06	3	25	$1.8 \times 10^8$	$5.9 \times 10^{35}$	0.5	$4 \times 10^8$	$5.2 \times 10^{32}$
	17:17:30	3	25	$1.6 \times 10^8$	$5.3 \times 10^{35}$	0.5	$10^8$	$1.3 \times 10^{32}$
	17:18:00	3	25	$1.6 \times 10^8$	$5.3 \times 10^{35}$	0.5	$4 \times 10^7$	$5.2 \times 10^{31}$
	17:18:30	3	25	$1.6 \times 10^8$	$5.3 \times 10^{35}$	0.5	$3 \times 10^8$	$3.9 \times 10^{32}$
	17:19:00	3	25	$1.5 \times 10^8$	$5.0 \times 10^{35}$	0.5	$2 \times 10^8$	$2.6 \times 10^{32}$
	17:19:30	3	30	$1.3 \times 10^8$	$6.1 \times 10^{35}$	0.45	$2 \times 10^8$	$2.2 \times 10^{32}$
	17:20:00	3	30	$1.3 \times 10^8$	$6.1 \times 10^{35}$	0.45	$1.3 \times 10^8$	$1.4 \times 10^{32}$
2003 11 4	17:21:00	3	32	$1.3 \times 10^8$	$7.0 \times 10^{35}$	0.38	$7 \times 10^7$	$5.3 \times 10^{31}$
	P1	2.3	40	$1.2 \times 10^6$	$1.0 \times 10^{34}$	0.5	$1.0 \times 10^{10}$	$1.0 \times 10^{34}$
	P2	2.3	40	$6.0 \times 10^5$	$5.0 \times 10^{33}$	0.25	$5.5 \times 10^9$	$1.8 \times 10^{33}$

1, which is close to the peak flux density of 11 000 sfu at 210 GHz for the October 28 burst, but the required electron number density for the November 4 burst is only  $10^{10} \text{ cm}^{-3}$  (see Table 3), which is only  $\sim 1/5$  of the required value ( $4.5 \times 10^{10} \text{ cm}^{-3}$ ) for the October 28 burst. In the decay phase the  $N$  and  $N_{\text{total}}$  values decreased about one and five times in the THz source, respectively.

#### 4.2 For the Steeply Rising THz Burst

A giant rising THz burst was detected on 2003 November 2 in the Super AR NOAA 10486. Observations show the flux density of the THz spectrum was steeply rising and the rising rate of the flux density of the THz spectrum attained a value as high as  $342 \text{ sfu GHz}^{-1}$  in the maximum phase. Its mean rising rate also reached a value of  $235 \text{ sfu GHz}^{-1}$  (corresponding to a spectral index  $\alpha$  of 4.8) during the burst (Li et al. 2016). The flux densities reached about 4000 and 70 000 sfu at 212 and 405 GHz at the maximum phase respectively. The emissions at 405 GHz maintained a continuous high level so that they largely exceeded the peak values of the MW spectra during the main phase. Our studies suggest that such a strong and steeply rising THz component can be produced by energetic electrons with a low-energy cutoff of 1 MeV via GS radiation in the case of a magnetic dipole field (Li et al. 2016). The electron number density  $N$ , derived from our numerical fits, increased substantially from  $8 \times 10^6$  to  $4 \times 10^8 \text{ cm}^{-3}$  at the rise phase, i.e., the  $N$  value increased 50 times at the rise phase (see Table 3). During the decay phase it decreased to  $7 \times 10^7 \text{ cm}^{-3}$ , i.e., it decreased by about five times from the maximum phase. The total electron number decreased an order of magnitude at the decay phase. Nevertheless in the MW emission source the  $N$  value only decreased by  $\sim 30\%$  and the total electron number did not decrease but rather increased by  $\sim 20\%$  at the decay phase.

The fit parameters at the maximum phase for the three radio events are given in Table 4. They indicate that the required electron number density reaches  $\sim 10^{10} \text{ cm}^{-3}$  for the two slowly rising THz burst spectra at the maximum phase, which is two orders of magnitude higher than that for the steeply increasing one. However, the steeply rising

THz spectrum requires a much higher low-energy cutoff of 1 MeV, but the two slowly rising THz burst spectra only require a 30 keV low-energy cutoff.

### 5 THE ENERGY FLUX OF ENERGETIC ELECTRONS

The energy flux and energy released by energetic electrons are important constraints on acceleration mechanisms (Miller et al. 1997). These quantities are sensitive to the low-energy cutoff in the electron distribution (Holman 2003). Once the energy cutoffs and the number density of the energetic electrons are obtained from the numerical fit of an observational spectrum, the distribution function of energetic electron  $n(E) = GE^{-\delta}$  and the instantaneous energy flux  $E_F$  carried by energetic electrons can be determined as well. Here we will present a formula that can be used to calculate  $E_F$  at any time, including the relativistic correction factor  $\gamma$  (Lorentz factor) (c.f. Zhou et al. 2011). It is

$$E_F \simeq \frac{3.0 G}{2.5 - \delta} (E_m^{2.5-\delta} - E_0^{2.5-\delta}) \gamma \quad (\delta \neq 2.5),$$

$$E_F \simeq 3.0 G \ln(E_m/E_0) \gamma$$

$$(\text{erg cm}^{-2} \text{ s}^{-1}) (\delta = 2.5). \quad (1)$$

The  $G$  factor is

$$G = \frac{N(\delta - 1)}{(E_0^{1-\delta} - E_m^{1-\delta})} \quad (\delta \neq 1),$$

$$G = N / \ln(E_m/E_0) \quad (\delta = 1). \quad (2)$$

Lorentz factor  $\gamma$  is a function of electron energy. Here it is taken as 2 and 7.3 corresponding respectively to 500 keV and 3.2 MeV for the two slowly and one steeply rising THz bursts. Then we can estimate the instantaneous energy flux  $E_F$  at the maximum time by putting these electron parameters (see Table 4) into Equations (1) and (2). The energy loss rate from the GS radiation,  $E' \text{ erg s}^{-1} (= E_F \times A)$ , can be estimated on the the source area  $A$ . Finally, the energy  $E$ , expressed in  $\text{erg s}^{-1} (= E' \times \Delta T)$ , released by energetic electrons via the GS radiation can also be calculated based on the lifetime  $\Delta T$  (expressed in s),

which represents the full width at half maximum for the burst time profile. The estimated energy flux, energy loss rate and energy released by energetic electrons are given in Table 5, corresponding to the THz and MW sources for the three bursts based on the physical parameters shown in Table 4.

Table 5 shows that the energy flux  $E_F$  carried by the energetic electrons reached  $1.5 \times 10^{15}$ ,  $8 \times 10^{14}$  and  $1.4 \times 10^{14}$  erg cm $^{-2}$  s $^{-1}$  at the maximum phase in the THz source for the three bursts, respectively. However in the MW source they only reached  $2.4 \times 10^{11}$ ,  $6.6 \times 10^{10}$  and  $1.8 \times 10^9$  erg cm $^{-2}$  s $^{-1}$  respectively, which are 3-5 orders of magnitude lower than those in the THz source. The energy loss rate  $E'$  reached ranges of  $6.1 \times 10^{30}$  –  $5.7 \times 10^{29}$  and  $4.8 \times 10^{28}$  –  $2.5 \times 10^{30}$  erg s $^{-1}$  respectively in the THz source and in the MW source at the maximum phase. It is found from Table 5 that although the modeled submillimeter source area is 3-4 orders of magnitude smaller than the modeled MW source, the energy ( $E_{\text{THz}}$ ) released by energetic electrons in the THz emission source still exceeds that ( $E_{\text{MW}}$ ) in the MW source. The ratio of  $E_{\text{THz}}$  to  $E_{\text{MW}}$  is 2.4, 5.0 and 12 for the three events, respectively. The total energy  $E_R$  released by energetic electrons in THz and MW sources reached  $3.8 \times 10^{33}$ ,  $1.6 \times 10^{33}$  and  $1.8 \times 10^{32}$  erg for the October 28 burst, and November 2 and 4 bursts, respectively (see Table 6). So considering the radio energy, the October 28 burst is the strongest of the three events.

## 6 DISCUSSION

### 6.1 Propagation Effect

Although flux density at 210 GHz of the October 28 burst is smaller than the corresponding value at 212 GHz of the November 4 burst, the required electron number density reaches as high as  $4.5 \times 10^{10}$  cm $^{-3}$ , which is 3.5 times higher than that of the November 4 burst, maybe due to the propagation effect. It was found that the emissivity of GS radiation increases with the propagation angle for the same harmonic number in the MW and millimeter range. Also, the increasing trend becomes more obvious (Zhou et al. 1999). In the THz range the propagation effect can be clearly identified in Figure 2. It shows the different GS emission spectra in the case of different propagation angles  $\theta$ , where  $\delta = 3$ ,  $E_0 = 500$  keV,  $E_m = 10$  MeV and  $N = 10^7$  cm $^{-3}$ . We can see from it that the flux densities at the higher frequencies in the THz range for  $\theta = 80^\circ$  are, at least, one order of magnitude higher than those for  $\theta = 20^\circ$ . The propagation effect results in a higher electron number density requirement under the quasi-longitudinal propagation than that under the quasi-transverse one for the same observational flux density distribution.

### 6.2 Variation in Source Size

We find that all the flux densities decreased rapidly in the THz range at the decay phase for the three THz bursts. If we still take the same source size ( $R = 0.5''$ ), then the

required electron number  $N$  will largely decrease, which leads to the modeled flux densities of the GS emission at 345 or 405 GHz always being lower than the observational results, i.e., the modeled rising rate is smaller than the observational one, so that the modeled GS spectrum cannot fit the observational spectrum at higher frequencies. In this case we have to take a smaller source size of  $0.38''$ ,  $0.35''$ , or even  $0.25''$  to fit these spectra in the decay phase for the three THz bursts, i.e., the THz source radius decreased by 20%–50% in the decay phase. The effect of the emission source size on the GS emission spectrum in the THz range is given (Li et al. 2016). On the contrary, we also found that the MW source size obtained from the spectral fit increased from  $25''$  to  $32''$  at the decay phase of the November 2 burst, i.e., the MW source radius increased by 28%. This variation in source size is perhaps a rather interesting result. It would be a reflection of the various changes from the energetic electron acceleration, trapping and the magnetic field topology in the burst source.

### 6.3 Comparison of Radio Energy and Thermal Energy

The energy  $E_{\text{THz}}$  and  $E_{\text{MW}}$  released by energetic electrons during the October 28 burst in the THz and MW ranges can attain values of  $2.7 \times 10^{33}$  and  $1.1 \times 10^{33}$  erg, respectively, which are the highest for the three bursts. The total radio energy  $E_R$  in the THz and MW ranges of the burst can reach  $3.8 \times 10^{33}$  erg due to a hard electron spectral index of 2 and a high electron number density of  $4.5 \times 10^{10}$  cm $^{-3}$  (see Table 4). So considering the radio energy, the October 28 burst is the strongest for the three events. The ratio of the radio energy to the thermal energy,  $E_R/E_T$ , is 131 for the October 28 burst, i.e., the radio energy is two orders of magnitude higher than the thermal energy estimated from the soft X-ray GOES observations of the emission measure and temperature. For the November 2 burst,  $E_{\text{THz}}$  only reached  $1.3 \times 10^{33}$  erg due to a narrower range of energy released by electrons, from 1 to 10 MeV and the mean electron number density. The value of  $E_R/E_T$  is 76 for this burst. For the November 4 burst the  $E_R/E_T$  value is only 4, because it is associated with the largest soft X-ray flare so far and the estimated thermal energy attained a value of  $5.2 \times 10^{31}$  erg.

### 6.4 Comparison of the Modeled Spectra from the Three Radio Bursts

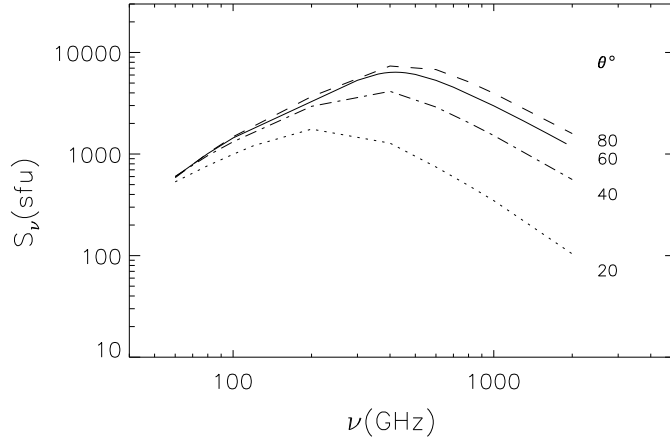
Figure 3 shows a comparison of the three modeled GS spectra fitting the observations of the October 28 and November 2 and 4 bursts over the interval of the maximum phase or at the maximum phase. It shows that the MW emission of the October 28 burst is the strongest for the three bursts, because it is produced by energetic electrons with a harder spectral index ( $\delta = 2$ ). However, the THz emission of the October 28 burst appears to be lower, although the observational flux density at 210 GHz is close to that of the other two bursts. It results from the correspond-

**Table 4** Parameters of the Burst Sources and Energetic Electrons at the Maximum Phase for the Three Rising THz Bursts

Date	$B_0$ (G)	$\theta^\circ$	$R''$	$\delta$	$E_0$ (keV)	$E_m$ (MeV)	$N$ ( $\text{cm}^{-3}$ )	$N_{\text{total}}$
2003 10 28 (THz)	5000	10	0.5	2.0	30	10	$4.5 \times 10^{10}$	$5.9 \times 10^{34}$
11 02	5000	60	0.5	3.0	1000	10	$4 \times 10^8$	$5.2 \times 10^{32}$
11 04	5000	80	0.5	2.3	30	10	$10^{10}$	$1.3 \times 10^{34}$
2003 10 28 (MW)	2800	10	25	2.0	10	5	$6 \times 10^7$	$2.0 \times 10^{35}$
11 02	2800	60	25	3.0	10	5	$1.8 \times 10^8$	$5.9 \times 10^{35}$
11 04	2000	80	40	2.3	10	5	$1.2 \times 10^6$	$1.0 \times 10^{34}$

**Table 5** Energy Flux  $E_F$ , Energy Loss Rate  $E'$  and Total Energy  $E$  Carried by Energetic Electrons via the GS Radiation in the THz and MW Sources for the Three Submillimeter Bursts

Date	$N$ ( $\text{cm}^{-3}$ )	$E_F$ ( $\text{erg cm}^{-2}\text{s}^{-1}$ )	$E'$ ( $\text{erg s}^{-1}$ )	$\Delta T$ (s)	$E$ (erg)
2003 10 28 (THz)	$4.5 \times 10^{10}$	$1.5 \times 10^{15}$	$6.1 \times 10^{30}$	450	$2.7 \times 10^{33}$
11 02	$4.0 \times 10^8$	$8.0 \times 10^{14}$	$3.3 \times 10^{30}$	380	$1.3 \times 10^{33}$
11 04	$10^{10}$	$1.4 \times 10^{14}$	$5.7 \times 10^{29}$	300	$1.7 \times 10^{32}$
10 28 (MW)	$6 \times 10^7$	$2.4 \times 10^{11}$	$2.5 \times 10^{30}$	450	$1.1 \times 10^{33}$
11 02	$1.8 \times 10^8$	$6.6 \times 10^{10}$	$6.9 \times 10^{29}$	380	$2.6 \times 10^{32}$
11 04	$1.2 \times 10^6$	$1.8 \times 10^9$	$4.8 \times 10^{28}$	300	$1.4 \times 10^{31}$

**Fig. 2** The effect of the propagation angles  $\theta^\circ$  on the GS emission spectrum in the submillimeter range, where  $\delta = 3$ ,  $E_0 = 500$  keV,  $E_m = 10$  MeV,  $N = 10^7 \text{ cm}^{-3}$  and  $B_0 = 5000$  G.

ing higher frequency ( $\nu > 210$  GHz) observations that have not been obtained during the main phase, so we only give an increasing THz spectral component with a smaller rising rate, which leads to an underestimated model spectrum. For the November 2 burst the modeled THz emission is the strongest among the three bursts and this peak frequency reaches 1440 GHz, due to intense ultrarelativistic electron GS radiation in a higher energy emission range of 1–10 MeV under the condition of quasi-transverse propagation. It is shown from the comparison of the modeled spectra of the three THz bursts that the emission strengths are very different for the three bursts and for the different emission frequency ranges, which strongly depend on the electron acceleration and various physical conditions of the burst region.

## 7 CONCLUSIONS

In the paper we investigate the three novel rising submillimeter bursts occurring in the Super AR NOAA 10486.

It is found from the numerical fit that the two slowly rising and one steeply rising submillimeter spectral components can be produced, respectively, by energetic electrons with energy ranges of 30 keV–10 MeV and 1–10 MeV in a compact source (having a radius of about  $0.5''$ ) with strong local magnetic fields varying from 4590 to 780 G via the GS emission. The photospheric magnetic field of 5000 G would be possible in an observation of a compact source (Li et al. 2016). The associated microwave spectral components can be produced by energetic electrons with 10 keV–5 MeV and with a mean local magnetic field strength in an extended source with a radius of  $25''$ – $40''$ .

It is found from the spectral temporal evolution that the variation amplitude in number density is much larger in the THz source than in the MW source during the bursts. The dramatic variation of electron number density in the THz source could result from the effective electron acceleration in the rise phase and strong electron energy loss during the flare, while in the MW source the variation amplitude of electron number density is one order of mag-

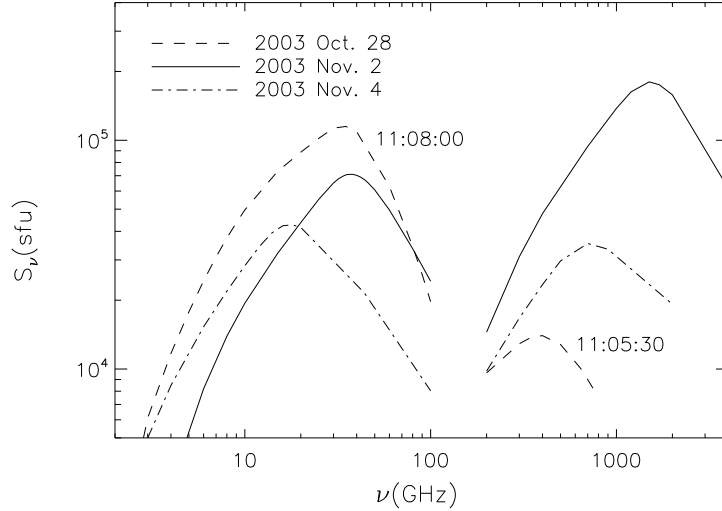


**Fig. 3** The modeled spectra for the observations at 11:08:00 and 11:05:30 UT over the interval of the maximum phase of the 2003 October 28 burst, at 17:17:06 UT of the maximum phase of the November 2 burst, and at peak 1 of the maximum phase of the November 4 burst (Zhou et al. 2011).

**Table 6** Total Radio Energy  $E_R$  (erg) Carried by Energetic Electrons and the Thermal Energy  $E_T$  (erg) Estimated from the Soft X-Ray GOES Observations

Date	$E_{\text{THz}}$ (erg)	$E_{\text{MW}}$ (erg)	$E_{\text{THz}}/E_{\text{MW}}$	$E_R$ (erg)	$E_T$ (erg)	$E_R/E_T$
2003 10 28	$2.7 \times 10^{33}$	$1.1 \times 10^{33}$	2.4	$3.8 \times 10^{33}$	$2.9 \times 10^{31}$	131
11 02	$1.3 \times 10^{33}$	$2.6 \times 10^{32}$	5.0	$1.6 \times 10^{33}$	$2.1 \times 10^{31}$	76
11 04	$1.7 \times 10^{32}$	$1.4 \times 10^{31}$	12	$1.8 \times 10^{32}$	$5.2 \times 10^{31}$	4

nitude lower than that in the THz source. This is because in the MW source there are much more electrons that decay from higher energy to lower energy and less electron energy loss. The instantaneous energy flux of electrons in the THz source is about 4–5 orders of magnitude higher than that in the MW source for the three bursts. Although the modeled THz source area is 3–4 orders of magnitude smaller than the modeled MW one, the energies released by energetic electrons in the THz source are 2–12 times those in the MW source due to the strong GS radiation loss at submillimeter wavelengths. The total energies released by energetic electrons via the GS radiation in the MW and THz sources are estimated, respectively, to be  $3.8 \times 10^{33}$ ,  $1.6 \times 10^{33}$  and  $1.8 \times 10^{32}$  erg for the October 28 and November 2 and 4 bursts, which are 131, 76 and 4 times as large as the thermal energies of  $2.9 \times 10^{31}$ ,  $2.1 \times 10^{31}$  and  $5.2 \times 10^{31}$  erg estimated from the soft X-ray GOES observations.

Our investigations show that the detailed GS emission models fit the rising submillimeter spectral components well for the three novel submillimeter bursts. So, this submillimeter spectral component could provide important diagnostics about the highly relativistic electrons with a higher energy range of a few tens of keV– $\sim 10$  MeV and their environment in the burst regions. Furthermore, it is found from the modeled calculations that the THz source radius decreased by 20%–50% during the decay

phase for the three events, but the MW source increased by 28% for the 2003 November 2 event. The interesting result about source size variations is perhaps significant for studies about energetic electron acceleration, trapping and variation in the magnetic field variation of the source region. However we must note that the required source radius is usually much smaller, based on the GS emission calculations. Further progress in understanding the physics of THz emission from flares requires more observations with a complete spectral coverage at the THz range, such as observations that can be acquired with the Atacama Large Millimeter/Submillimeter Array (ALMA).

**Acknowledgements** The authors thank Dr. V. F. Melnikov for fruitful discussions. This study is supported by the National Natural Science Foundation of China (Grant Nos. 11333009 and 11573072), and the “973” program (No. 2014CB744200).

## References

- Bastian, T. S., Benz, A. O., & Gary, D. E. 1998, *ARA&A*, 36, 131  
 Dulk, G. A. 1985, *ARA&A*, 23, 169  
 Holman, G. D. 2003, *ApJ*, 586, 606

- Kane, S. R., McTiernan, J. M., & Hurley, K. 2005, *A&A*, 433, 1133
- Kaufmann, P., Raulin, J.-P., de Castro, C. G. G., et al. 2004, *ApJ*, 603, L121
- Krucker, S., Giménez de Castro, C. G., Hudson, H. S., et al. 2013, *A&A Rev.*, 21, 58
- Li, J. P., Zhou, A. H., & Wang, X. D. 2016, *RAA (Research in Astronomy and Astrophysics)*, 16, 1, 008
- Lüthi, T., Lüdi, A., & Magun, A. 2004a, *A&A*, 420, 361
- Lüthi, T., Magun, A., & Miller, M. 2004b, *A&A*, 415, 1123
- Miller, J. A., Cargill, P. J., Emslie, A. G., et al. 1997, *J. Geophys. Res.*, 102, 14631
- Pick, M., Klein, K.-L., & Trottet, G. 1990, *ApJS*, 73, 165
- Ramaty, R., Schwartz, R. A., Enome, S., & Nakajima, H. 1994, *ApJ*, 436, 941
- Silva, A. V. R., Share, G. H., Murphy, R. J., et al. 2007, *Sol. Phys.*, 245, 311
- Trottet, G., Krucker, S., Lüthi, T., & Magun, A. 2008, *ApJ*, 678, 509
- Zhou, A.-H., Huang, G.-L., & Wang, X.-D. 1999, *Sol. Phys.*, 189, 345
- Zhou, A. H., Li, J. P., & Wang, X. D. 2008, *Sol. Phys.*, 247, 63
- Zhou, A. H., Huang, G. L., & Li, J. P. 2010, *ApJ*, 708, 445
- Zhou, A. H., Li, J. P., & Wang, X. D. 2011, *ApJ*, 727, 42